

PREDICTION OF ACOUSTIC WAVE PROPAGATION IN THE VICINITY OF A WEDGE COSTAL REGION USING AN EFFICIENT NUMERICAL MODEL

E. G. A. Costa^a, L. M. C. Godinho^b, A. S. C. Pereira^b, J. A. F. Santiago^a and R. Dias^a

^a*COPPE/Federal University of Rio de Janeiro, Department of Civil Engineering, Caixa Postal 68506, CEP 21945-972, Rio de Janeiro, RJ, Brazil, edundo_costa@coc.ufrj.br, santiago@coc.ufrj.br, rodrigodias@coc.ufrj.br, <http://www.coc.ufrj.br/>*

^b*CICC, Department of Civil Engineering, University of Coimbra, Pinhal de Marrocos, 3030-788, Coimbra, Portugal, lgodinho@dec.uc.pt, apereira@dec.uc.pt, <http://www.dec.uc.pt>*

Keywords: Method of Fundamental Solutions, Green's Function, Shallow water.

Abstract. Different boundary-only numerical frequency domain formulations are here developed and applied to simulate the two-dimensional (2D) acoustic wave propagation in the vicinity of a underwater configuration. This configuration combines two sub-regions, one of them being a wedge with rigid bottom and free surface, and the second one being a waveguide with a rigid flat bottom and a free flat surface. Both the Boundary Element Method (BEM) and the Method of Fundamental Solutions (MFS) are used to solve this problem. In either cases, Green's functions that take into account the presence of flat rigid and free surfaces of the waveguide and of a wedge are used. A sub-region technique is used to connect the two parts of the domain, enforcing continuity of the relevant quantities. The Green's functions are defined using two approaches: the image source method is used to model the rigid flat bottom and free flat interface, whereas the response provided by the wedge sub-region is based on a normal mode solution. A third boundary element formulation is also considered, which makes use of Green's functions for a perfect waveguide (using the image source method), therefore requiring the discretization of the sloping rigid bottom of the wedge. The presented formulations are discussed, both in what concerns accuracy and computational effort. The results obtained by the authors indicate that the MFS has a significantly lower computational cost and is very stable, therefore being adequate for the analysis of acoustic wave propagation in the studied configurations.

1 INTRODUCTION

Over the years, different computational methods have been proposed to determine the sound field in an underwater acoustic environment. Many methods have been applied with success, as documented in the reference work of Jensen et al. (2000), but all of them with specific drawbacks and limitations. In ocean acoustics, some of the most widely used methods are based on acoustic ray theory, normal mode analysis (first applied by Pekeris (1948)), parabolic equations (introduced first by Hardin and Tappert (1973)) or Green's functions for layered media (such as those defined by Schmidt and Tango (1986) or Tadeu et al. (2000) and Tadeu et al. (2005)).

Modern high-speed computing infrastructures allowed the development of different and more accurate approaches based on the wave theory for some specific problems in underwater acoustics. Among those approaches are finite difference, finite element and boundary element numerical methods.

Santiago and Wrobel (1999) and Santiago and Wrobel (2000) implemented the sub-region technique in a boundary element formulation for the analysis of two-dimensional acoustic wave propagation in a shallow water region with irregular seabed topography. In their approach the bottom and surface boundaries of the regions are modeled using Neumann and Dirichlet conditions, allowing for the use of Green's functions that satisfy either the free surface boundary condition or both the boundary conditions on the free surface and rigid bottom.

In many cases, the geometry of the propagation domain can be assumed to be constant in one direction; additionally, if the acoustic excitation is modeled as a three-dimensional (3D) source, these problems are usually called 2.5D, and the 3D acoustic wave equation can be mathematically manipulated to obtain the frequency-domain solution as a summation of simpler 2D problems (Bouchon and Aki, 1977). Boundary element models have been developed using this technique to compute the pressure field in ocean environments (Branco et al., 2002, Godinho et al., 2001)

When complex geometries are analyzed, boundary element methods may present specific problems, since it may become necessary to perform large discretization schemes, leading to high computational effort. One way of avoiding these large discretizations is incorporating appropriate Green's functions to account for part of the boundaries, such as a free surface.

Meshless methods have, in recent years, received the attention of scientists and researchers. These methods do not require explicit domain or boundary discretization. One such technique is the Method of Fundamental Solutions (MFS) (Golberg et al., 1999, Cho et al., 2004). Mathematically, the MFS is a rather simple technique, but it requires previous knowledge of the Green's functions of the propagation domains. Despite of the potential interest in developing those techniques to treat underwater wave propagation problems, very little can be found in the literature. The use of such methods together with Green's functions that automatically satisfy specific boundary conditions may be a further interesting option.

In the present paper the authors aim to analyze the efficiency and accuracy of different numerical formulations developed to allow for the computation of the acoustic wave propagation in a specific underwater acoustics configuration. These formulations may incorporate Green's functions that allow reducing the discretization needs. Two different numerical methods are used here: the first one is the BEM and the second is the MFS. In all cases, the analyzed region is assumed to be two-dimensional, simulating underwater acoustic problems which have little variation in the long shore direction, and is divided in two sub-regions: the first one is a flat waveguide, composed of a flat rigid bottom and a flat free

surface; the second is defined by a wedge, with rigid bottom and free surface.

Three formulations are discussed. The first two are based on BEM and MFS models, respectively, requiring the definition of two sub-domains where appropriate Green's functions can be determined, and thus only requiring the interface between sub-regions to be discretized. In the first sub-domain, which assumes a flat rigid bottom and a flat free surface, Green's functions obtained using the Image Source Method are used. In the second one, defining a wedge, the Green's functions are obtained using an approach based on the sum of normal modes (Buckingham and Tolstoy, 1990). The third model also makes use of the BEM, but requires discretization of the inclined rigid bottom that forms the wedge. This model assumes only one region and makes use of adequate Green's functions based on the Image Source Method.

This paper is organized as follows: first, the mathematical formulation of the problem is presented, including a brief description of the BEM formulation and of the MFS; the Green's functions used are then defined, followed by a convergence analysis performed for the case of the wedge; after this, the proposed models are verified by comparing the results they provide against each other; the performance and accuracy of the three models is then discussed; finally, a numerical application is presented.

2 PROBLEM FORMULATION

Consider the problem of acoustic wave propagation in a region Ω of infinite extent along the z direction, with irregular rigid seabed topography and flat free surface, as shown in Figure 1.

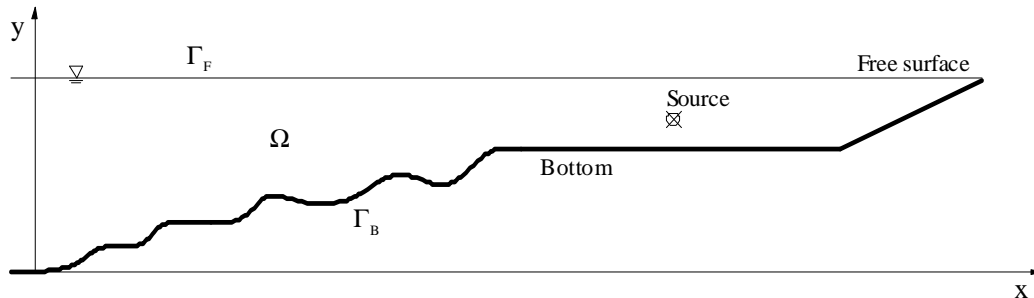


Figure 1: Geometry of the problem.

If the source of acoustic disturbance is time-harmonic, the sound velocity is constant and the medium in the absence of perturbations is quiescent, the governing Helmholtz equation for this problem can be written as:

$$\nabla^2 \phi + k^2 \phi = -\sum_{l=1}^{NS} Q_l \delta(\xi_l^f, \xi), \quad \text{in region } \Omega \quad (1)$$

where NS is the number of sources in domain; ϕ is the velocity potential; Q_l is the magnitude of the existing sources ξ_l^f located at $(x_{\xi_l^f}, y_{\xi_l^f})$; ξ is a domain point located at (x_ξ, y_ξ) ; $\delta(\xi_l^f, \xi)$ is the Dirac delta generalized function; and $k = \omega/c$ is the wave number, with ω being the angular frequency and c the speed of sound in the medium.

In this problem the following conditions were prescribed: the Dirichlet condition in the boundary of the free surface Γ_F ; Neumann condition in the boundary of the bottom Γ_B and

Sommerfeld radiation condition at infinity.

To solve this problem, two numerical strategies are used in this paper, and are presented in the following sections.

2.1 Boundary Element Method

To solve the proposed problem using the BEM together with full-space Green's functions requires discretization of all surfaces. Here, however, we will make use of Green's functions that satisfy specific boundary conditions allowing for reduction of boundary discretization. The formulations that will be described refer to the specific geometry of a shallow water configuration which combines two sub-regions, one with flat surfaces and a second corresponding to a wedge region as defined in Figure 2, excited by a linear load.

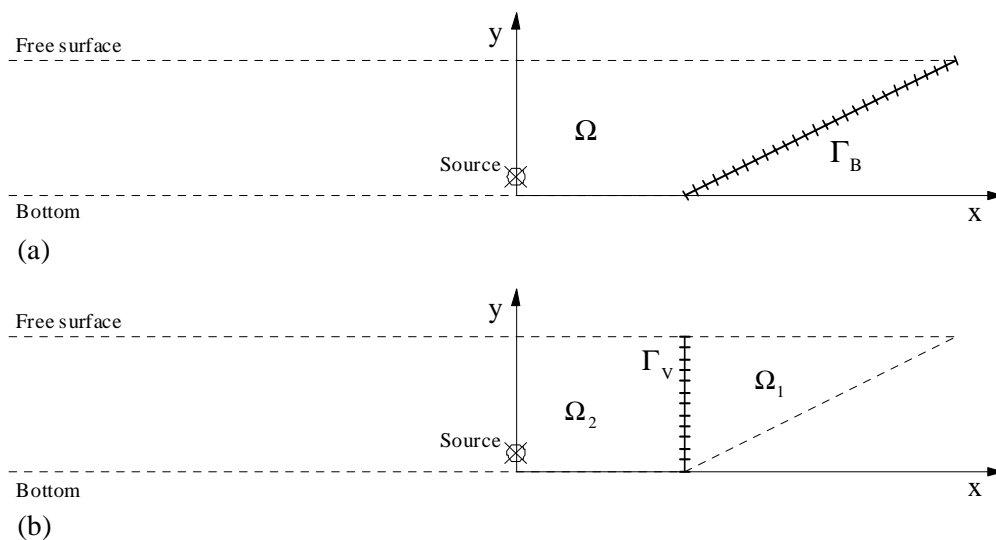


Figure 2: Geometry of the BEM models: (a) Model 1; (b) Model 2.

Two different models are here proposed: one (Model 1) makes use of a Green's function that directly satisfies the boundary conditions in the flat rigid bottom and flat free surface, requiring only the discretization of the sloping bottom of the wedge (see Figure 2a); the second model (Model 2) makes use of two different types of Green's functions, and therefore a sub-region technique is applied by defining two regions, with only the interface in-between requiring discretization (see Figure 2b).

Considering Model 1 excited by a unit load ξ^f , if we introduce the appropriate boundary conditions at the discretized sloping bottom Γ_B , and assuming NE_B constant elements with linear geometry, by applying the collocation method to the integral equation, in terms of an intrinsic coordinate η , the following equation may be obtained:

$$C(\xi_p)\phi(\xi_p) = -\sum_{q=1}^{NE_B} \int_{-1}^1 \frac{\partial G^{f^{rb}-f^{fs}}(\xi_p, \mathbf{x}_q)}{\partial n} \phi(\mathbf{x}_q) |J| d\eta + G^{f^{rb}-f^{fs}}(\xi^f, \xi_p), \quad (2)$$

where ξ_p refers to the functional node p with p ranging from 1 to NE_B ; $|J|$ is the Jacobian; $\phi(\mathbf{x}_q)$ is the unknown velocity potential at the boundary element \mathbf{x}_q ; $G^{f^{rb}-f^{fs}}(\xi_p, \mathbf{x}_q)$ is the fundamental solution for a waveguide with flat rigid bottom and free surface at the boundary

element \mathbf{x}_q , whose details are given in a subsequent section; $G^{frb-ffs}(\xi^f, \xi_p)$ is the incident field regarding the velocity potential generated by the real source placed at position ξ^f .

Solving the resulting system of $N_{EB} \times N_{EB}$ equations makes it possible to obtain the nodal solid velocity potentials at the sloping bottom Γ_B . The scattered wave field at any point of the domain can then be calculated by applying the Boundary Integral equation.

If, as in Model 2, we use a Green's function that satisfies the boundary conditions of the wedge, only the interface Γ_v between the flat waveguide and the wedge needs to be discretized (see Figure 2b), requiring a substantially lower number of boundary elements to be used if analyzing wedges with small apex angles and greater lengths.

In these conditions (Model 2), if we introduce the appropriate boundary conditions at the discretized interface Γ_v (which are continuity of velocity potentials and continuity of the normal derivative of the velocity potentials), and assuming NE_v constant elements with linear geometry, by applying the collocation method to the integral equation, in terms of an intrinsic coordinate η , the following equations may be obtained:

- Region Ω_1

$$C(\xi_p)\phi(\xi_p) = \sum_{q=1}^{NE_v} \int_{-1}^1 G^{wrb-wfs}(\xi_p, \mathbf{x}_q) \frac{\partial \phi}{\partial \mathbf{n}}(\mathbf{x}_q) |J| d\eta - \sum_{q=1}^{NE_v} \int_{-1}^1 \frac{\partial G^{wrb-wfs}(\xi_p, \mathbf{x}_q)}{\partial \mathbf{n}} \phi(\mathbf{x}_q) |J| d\eta + (1 - \vartheta) G^{wrb-wfs}(\xi^f, \xi_p) \tag{3}$$

- Region Ω_2

$$C(\xi_p)\phi(\xi_p) = \sum_{q=1}^{NE_v} \int_{-1}^1 G^{frb-ffs}(\xi_p, \mathbf{x}_q) \frac{\partial \phi}{\partial \mathbf{n}}(\mathbf{x}_q) |J| d\eta - \sum_{q=1}^{NE_v} \int_{-1}^1 \frac{\partial G^{frb-ffs}(\xi_p, \mathbf{x}_q)}{\partial \mathbf{n}} \phi(\mathbf{x}_q) |J| d\eta + \vartheta G^{frb-ffs}(\xi^f, \xi_p) \tag{4}$$

In Eqs. (3) and (4), $\phi(\mathbf{x}_q)$ and $\partial\phi/\partial n(\mathbf{x}_q)$ represent, respectively, the unknown velocity potential and its normal derivative at point \mathbf{x}_q ; the Green's function $G^{wrb-wfs}(\xi_p, \mathbf{x}_q)$ directly satisfies the wedge surfaces' conditions; $\vartheta=1$ if the source is positioned in region Ω_2 , while $\vartheta=0$ if the source is placed in region Ω_1 .

Solving the resulting system of $2N_{EV} \times 2N_{EV}$ equations makes it possible to obtain the relevant unknowns at the vertical interface Γ_v .

2.2 Method of Fundamental Solutions

An approximate solution for the Helmholtz equation (Eq. (1)) can also be obtained by making use of the MFS. In this method, the solution at an internal point of the domain is obtained in terms of a linear combination of fundamental solutions centered on NFS virtual sources, placed outside the region of interest.

The model developed in this article (designated by Model 3) using the MFS assumes an

acoustic domain divided into two sub-regions, as illustrated in Figure 3, allowing the use of two different Green’s functions: in region Ω_1 a fundamental solution that directly satisfies the rigid bottom and free surface wedge conditions is assumed, whereas in region Ω_2 a solution that directly satisfies the rigid and free flat surface conditions is used. With this procedure, a fictitious vertical interface is defined using a number of NFS collocation points (displayed in Figure 3). A total of $2NFS$ fictitious sources must then be used to define the velocity potential field at both regions.

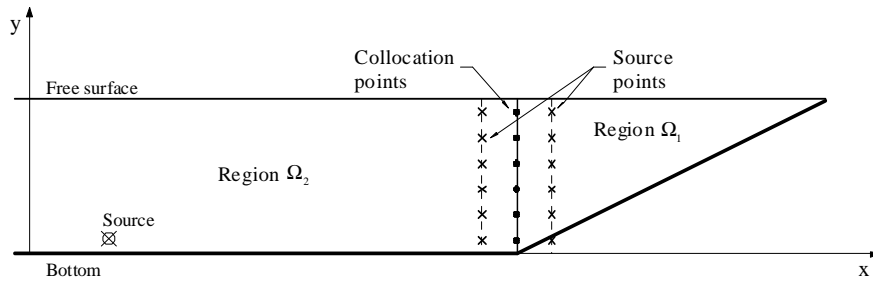


Figure 3: Geometry of the MFS model.

For each region, the velocity potential can then be written as:

$$\phi(\mathbf{x}) = \sum_{n=1}^{NFS} \mathbf{A}_n G^{wrb-wfs}(\xi_n, \mathbf{x}) + (1 - \vartheta) G^{wrb-wfs}(\xi^f, \mathbf{x}) \quad \text{region } \Omega_1 \quad (5a)$$

$$\phi(\mathbf{x}) = \sum_{n=1}^{NFS} \mathbf{B}_n G^{frb-ffs}(\xi_n, \mathbf{x}) + \vartheta G^{frb-ffs}(\xi^f, \mathbf{x}) \quad \text{region } \Omega_2 \quad (5b)$$

where ξ^f is the coordinate (x_{ξ^f}, y_{ξ^f}) of the real source position; ξ_n refers to the coordinate of the n^{th} virtual source point placed along a fictitious boundary; A_n and B_n are the amplitudes to be determined for each of the $2NFS$ source points; $\vartheta=1$ if the source is positioned in region Ω_2 and $\vartheta=0$ if the source is placed in region Ω_1 ; $G^{wrb-wfs}(\xi^f, \mathbf{x})$ is the incident field regarding the velocity potential generated by the real source when placed in the wedge region and $G^{frb-ffs}(\xi^f, \mathbf{x})$ regards the incident field generated by the real source when placed in the flat region; NFS corresponds to the number of sources placed at each sub-region; $G^{frb-ffs}(\xi_n, \mathbf{x})$ refers to the Green’s function for a flat rigid bottom and a flat free surface and $G^{wrb-wfs}(\xi_n, \mathbf{x})$ regards the Green’s function for a wedge region with free surface and rigid bottom whose details are given in the next section. By adequately deriving the Eqs. (5a) and (5b), the normal derivative of the velocity potential may also be obtained.

If we impose, at each interface point x , continuity of the velocity potential and of its normal derivative, the following equations are obtained:

$$\sum_{n=1}^{NFS} \mathbf{A}_n G^{wrb-wfs}(\xi_n, \mathbf{x}) + (1 - \vartheta) G^{wrb-wfs}(\xi^f, \mathbf{x}) = \sum_{n=1}^{NFS} \mathbf{B}_n G^{frb-ffs}(\xi_n, \mathbf{x}) + \vartheta G^{frb-ffs}(\xi^f, \mathbf{x}) \quad (6a)$$

$$\sum_{n=1}^{NFS} \mathbf{A}_n \frac{\partial G^{wrb-wfs}(\xi_n, \mathbf{x})}{\partial \mathbf{n}} + (1-\vartheta) \frac{\partial G^{wrb-wfs}(\xi^f, \mathbf{x})}{\partial \mathbf{n}} = \sum_{n=1}^{NFS} \mathbf{B}_n \frac{\partial G^{fwb-ffs}(\xi_n, \mathbf{x})}{\partial \mathbf{n}} + \vartheta \frac{\partial G^{fwb-ffs}(\xi^f, \mathbf{x})}{\partial \mathbf{n}} \quad (6b)$$

By writing these equations for the NFS collocation points a linear system of $2NFS \times 2NFS$ equations is obtained. Once the system of equations is solved for the relevant unknowns, the response at any point of the domain may be obtained by using expressions (5).

3 FUNDAMENTAL SOLUTIONS

3.1 Analytical solution for a region with flat rigid and free surfaces

By applying the image source method one obtains a Green’s function, written as an infinite series of source terms, which directly satisfies both boundary conditions at the ocean rigid bottom and free flat surface. However, the truncation of the number of sources will lead to the exact satisfaction of only one boundary condition and the approximate satisfaction of the other. Therefore, two types of truncated series can be constructed (Santiago and Wrobel, 2000, Santiago and Wrobel, 2004).

In the present work, we deal with the solution that exactly satisfies the boundary conditions at the free surface, defined as $G_F^{fwb-ffs}(\xi, \mathbf{x})$, but which produces a very small non-zero value at the rigid boundary. This solution can be given as:

$$G_F^{fwb-ffs}(\xi, \mathbf{x}) = \frac{i}{4} \left\{ H_0^{(1)}(kr) - H_0^{(1)}(kr^{(1F)}) + \sum_{m=1}^{\infty} G_{F_m}(\xi, \mathbf{x}) \right\} \quad (7a)$$

$$G_{F_m}(\xi, \mathbf{x}) = (-1)^{m+1} \left[H_0^{(1)}(kr_m^{(2F)}) - H_0^{(1)}(kr_m^{(3F)}) - H_0^{(1)}(kr_m^{(4F)}) + H_0^{(1)}(kr_m^{(5F)}) \right], \quad (7b)$$

where the superscripts (jF) identify the reflected source points ($j=1 \dots 5$).

The distances from the field point \mathbf{x} to the source points $\xi^{(jF)}$ are denoted as r , $r^{(1F)}$ and $r_m^{(jF)}$. These distances can be written as: $r = |\mathbf{x} - \xi| = \sqrt{(x - x_\xi)^2 + (y - y_\xi)^2}$; $r^{(1F)} = |\mathbf{x} - \xi^{(1F)}| = \sqrt{(x - x_\xi)^2 + (y - y_\xi^{(1F)})^2}$ and $r_m^{(jF)} = |\mathbf{x} - \xi^{(jF)}| = \sqrt{(x - x_\xi)^2 + (y - y_{\xi_m}^{(jF)})^2}$ in which $y_\xi^{(1F)} = 2Y_F - y_\xi$; $y_{\xi_m}^{(2F)} = -2(m-1)Y_F + 2mY_B - y_\xi$; $y_{\xi_m}^{(3F)} = 2m(-Y_F + Y_B) + y_\xi$; $y_{\xi_m}^{(4F)} = 2m(Y_F - Y_B) + y_\xi$ and $y_{\xi_m}^{(5F)} = 2(m+1)Y_F - 2mY_B - y_\xi$. In these expressions, Y_F and Y_B refer to the y coordinate of the free surface and bottom, respectively.

It is worth noting that the above defined series exhibit a slow convergence, requiring a large number of terms to obtain the solution. However, this process can be greatly improved by using complex frequencies, with the form $\omega_c = \omega + i\zeta$, with ζ defining a damping effect (Kausel and Roesset, 1992). One additional advantage of using this damping factor is that it can also be used to remove aliasing effects when time-series are to be calculated from the frequency response. In the time domain, this damping is later taken into account by applying an exponential window $e^{\zeta t}$ to the response.

3.2 Analytical solution for an ideal wedge

The analytical solution for an ideal wedge, used in this paper, exactly satisfies the boundary condition on the flat free surface and on the sloping bottom of the wedge. This solution was obtained from the inhomogeneous Helmholtz equation and it is given by the following expression (Buckingham and Tolstoy, 1990, Jensen and Ferla, 1990, Stotts, 2002):

$$G^{wrb_wfs} = \frac{i\pi}{\theta_0} \sum_{m=1}^{\infty} J_{\nu}(kr_{<}) H_{\nu}^{(1)}(kr_{>}) \times \sin(\nu\theta) \sin(\nu\theta'), \quad (8)$$

where θ_0 is the wedge angle; J_{ν} is the Bessel function of the first kind of order ν ; $H_{\nu}^{(1)}$ is the Hankel function of the first kind of order ν ; $r_{<} = \min(r, r')$, $r_{>} = \max(r, r')$, with r and r' being the ranges of the receiver and source from the apex of the wedge; θ and θ' are the angular depths of the receiver and source measured about the apex; the orders of the Bessel and Hankel functions for rigid bottom are given by $\nu = (m - \frac{1}{2})\pi/\theta_0$.

It is important to note that this fundamental solution poses some difficulties in its implementation. In fact, when the real order ν becomes large in relation to the fixed argument κ , (i.e. when $\nu \rightarrow \infty$) the function $Y_{\nu}(\kappa) \rightarrow \infty$ while $J_{\nu}(\kappa) \rightarrow 0$. Noting that $Y_{\nu}(\kappa)$ is the Bessel function of second kind, which corresponds to the imaginary component of the Hankel function, the product between the Hankel function and the Bessel function of the first kind is the product of a very large number by a very small number. Fortran compilers, making use of double precision variables, may not have the required precision to compute this product, as necessary in Eq. (8). This may occur particularly when r and r' are very close to each other, for which a large number of terms (and very high order ν) becomes necessary to attain convergence. However, in the present work, the MFS is used to model the proposed system, and the source point is always positioned away from the receiver point (r and r' are markedly distinct). For this reason, the convergence of the solution occurs with a small number of terms and this fundamental solution presents a good behavior.

In order to understand the possible advantages of using this solution in either BEM or MFS models, convergence tests were performed. With this purpose a geometry was chosen which assumes a set of source and receiver' positions defined so that they would allow to understand the behavior of the function when implemented in BEM or MFS codes. The example refers to an ideal wedge, with sound velocity 1500ms^{-1} , subjected to a harmonic line source S1 applied at position (0.00m;19.00m) and to a second source (S2) applied at position (-5.00m;19.00m). The responses were computed at receiver R1 placed at (0.00m;19.20m) and at another receiver (R2) placed at point (0.00m;10.00m), as illustrated in Figure 4. In the analysis, complex frequencies with an imaginary part of ($\zeta = 0.7 \times 2 \times \pi \times \Delta f$) were used.

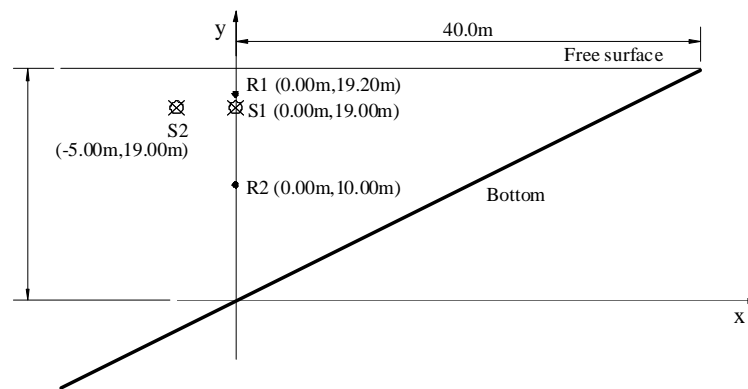


Figure 4: Geometry of the wedge used in the convergence tests.

The number of terms required to compute the Green' function for each frequency, in the range [4.0; 256 Hz], with a frequency step of 4.0 Hz, is evaluated. Figure 5 displays the obtained responses for receiver R1 and R2, respectively, when the source is either S1 or S2. From the analysis of this figure, which plots the number of terms required to achieve convergence for each frequency of the defined range, we conclude that the number of terms increases with the proximity between source and receiver. This behavior is consistent across the full frequency range. It is also clear, in those plots, that the number of terms needed for convergence when the source is at S1 and the receiver at R1 is very large (around 4000), and it decreases dramatically for all other cases.

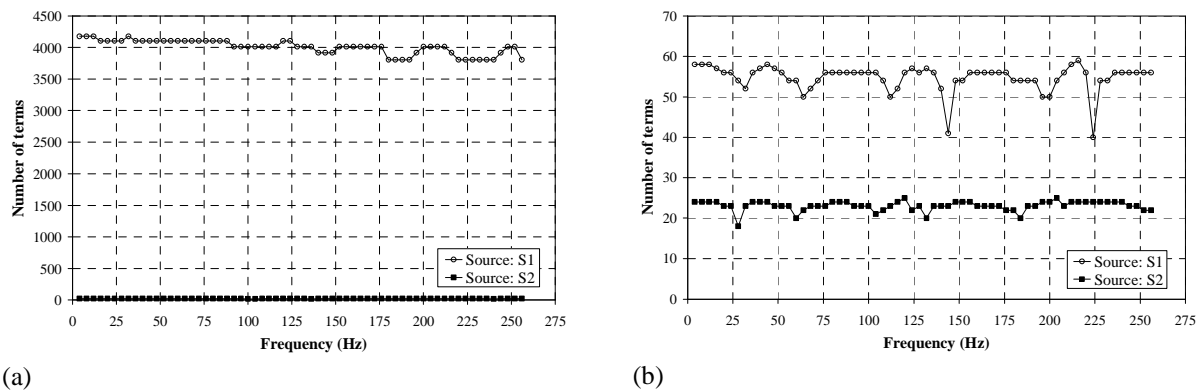


Figure 5: Number of terms responses as a function of the frequency range 4-256Hz: (a) receiver R1 and (b) receiver R2.

The described findings indicate that the implementation of this functions in a BEM code may poses difficulties, since it becomes time consuming to perform integrations over the loaded element, and thus with the loaded point very close to the receiver point. Additionally, it is important to note that the implementation of this function in the BEM models requires calculation of the Green's function integration when the functional point and the nodal point of the boundary element coincide, leading to a singularity. To avoid this problem, the integration was computed in two parts:

- numerical integration of the reflected field (using Gauss quadrature scheme), obtained from expression (8) by subtracting the incident field from the solution;
- analytical integration of the singular part, originated by the source using the expressions described by Tadeu et al. (1999 b,a).

In practice, subtracting the full-space Green's function from Eq. (8) removes its singularity, allowing for the numerical integration to be performed accurately.

4 BEHAVIOUR OF THE BEM AND MFS MODELS

The BEM and MFS algorithms used in this work were implemented and verified by comparing the results with a BEM model, where a 2D Green's function for full space is used (reference model). This model requires the discretization of both the bottom and the surface, while the BEM models defined earlier in this work need only the discretization of either the sloping bottom of the wedge (Model 1) or the vertical interface between sub-regions (Model 2), as illustrated in Figure 6. As for the MFS model (Model 3), collocation points at the interface and fictitious source points in each sub-region must be defined (see also Figure 3).

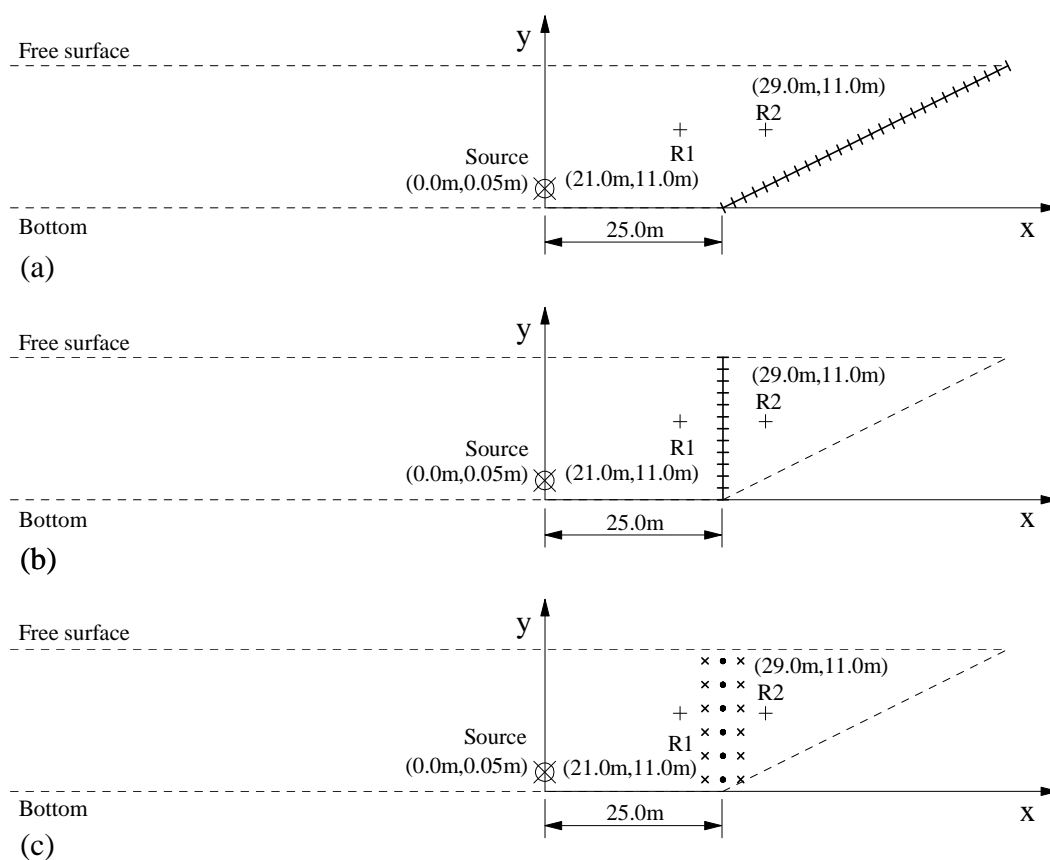


Figure 6: Geometry of the problem: (a) Model 1: geometry only with sloping bottom discretized (BEM); (b) Model 2: geometry with interface discretized (BEM); (c) Model 3: geometry only with collocation and fictitious points (MFS).

Consider, now, a propagation domain containing a fluid medium with a sound velocity of 1500ms^{-1} , and consisting of a flat waveguide 20.00m depth connected to a wedge region, 40.00m long, with an apex angle of 26.56° . The geometry was subjected to a harmonic line load applied near the rigid bottom at point $(0.00\text{m};0.05\text{m})$. The responses were calculated at receiver R2 placed at $(29.00\text{m};11.00\text{m})$, as illustrated in Figure 6. Computations are performed for frequencies up to 256.0 Hz , with a frequency step of 4.0 Hz . Complex frequencies with an imaginary part of $(\zeta = 0.7 \times 2 \times \pi \times \Delta f)$ were assumed. When using the BEM models the number of boundary elements is defined as a function of the frequency, by

using a relation between the incident wavelength and the length of the boundary element, equal to a minimum of 10. In Models 1 and 2, a minimum of 5 boundary elements was always adopted. As in the BEM models, the number of collocation points used in the MFS is computed using the same relation between the incident wavelength and the distance between collocation points. Additionally, for the MFS, the distance between the fictitious sources and the interface was fixed at 5 times the distance between interface points.

In order to illustrate the responses obtained in the verification, Figure 7 displays the velocity potential recorded at receiver R2 computed using the three models defined. In this figure the response provided by the reference BEM model is also included. Observation of those figures confirms the very good agreement among all solutions.

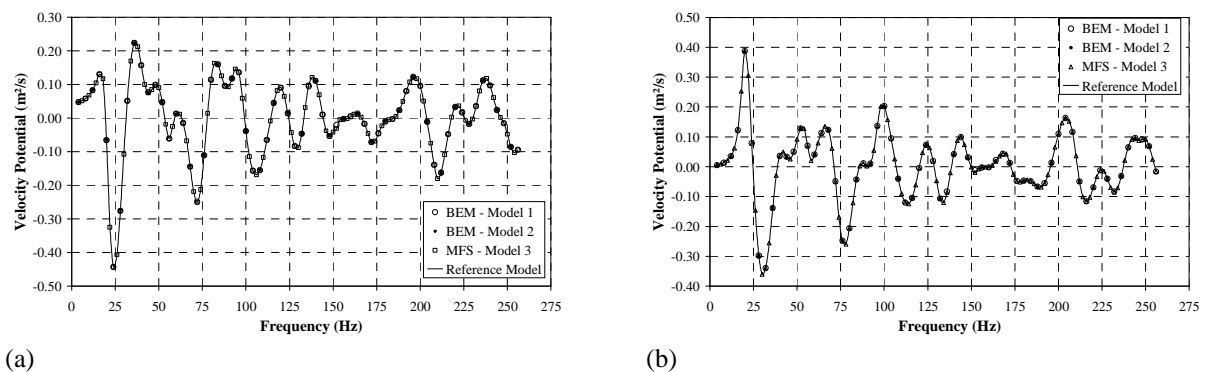


Figure 7: Verification of the problem for Receiver 2: (a) Real part; (b) Imaginary part.

It is important to state that additional tests were performed to understand the sensitivity of the MFS model with relation to the distance between the virtual sources and the interface. Those tests (not shown in this work) allowed concluding that there is very little variation of the response with this distance, and that relatively large distances (of the order of 10 times the distance between consecutive collocation points) may be used. Those relatively large distances can greatly help to improve the convergence of the fundamental solutions, and may render the method efficiency for the analysis of ocean acoustic problems with this geometry.

This efficiency has been analyzed comparing the computation times requires by the different models. Two different geometries were used, both with the same depth (20.00m) in the flat region and different wedge dimensions. The first geometry is the same as described above (wedge length of 40.00m), whereas in the second case, corresponding to a more realistic configuration, the wedge assumes a length of 200.00m, which leads to an apex angle of 5.71° . The calculations were performed assuming frequencies up to 256 Hz and a 2 Hz frequency step. Once again, the sound velocity of the fluid medium used was 1500ms^{-1} . The responses were computed in a computer with an AMD Turion (tm) 64 mobile technology ML-34 processor, with a clock frequency of 1.79GHz, and 1 GB of RAM. To ensure that comparable results were obtained, those computation times were obtained always using the same relation between the incident wavelength and the length of the boundary element for both BEM models, and also using the same relation to define the number of interface points for the MFS model. Relations of 5 and 10 are tested. Note that both the BEM and the MFS model display a good agreement with the reference solution even with a relation of 5 (not displayed).

Figure 8a displays the results obtained for the first geometry, while the corresponding responses for the second geometry are illustrated in Figure 8b. In these plots the computation

time provided by BEM - Model 2 was not included, because it is at least one order of magnitude higher than those obtained using BEM - Model 1 and MFS model (Model 3). This high computational time was expected, and is related to the slow convergence of the fundamental solution for the wedge geometry, when the source and receiver points are near each other, and over the same vertical line. This effect has been identified and illustrated in Section 3.

From the analysis of Figure 8 we observe that BEM Model 1 displays shorter computation times than those obtained using the MFS, denoting that for this geometry it is more efficient. Note that the peaks in the curve regarding the MFS model are related to computations of the Green's function used to model the wedge region, which significantly increase the computation times. When a larger wedge length is assumed (see Figure 8b), the MFS model becomes significantly more efficient than the BEM (Model 1 and Model 2), mainly as frequency increases, allowing to achieve shorter computation times. In fact, in this figure, the difference between computation times for the two models is striking, with the MFS model being about 10 times faster than the BEM when the number of points/elements is defined using a relation of 10, and even faster for the lower relation.

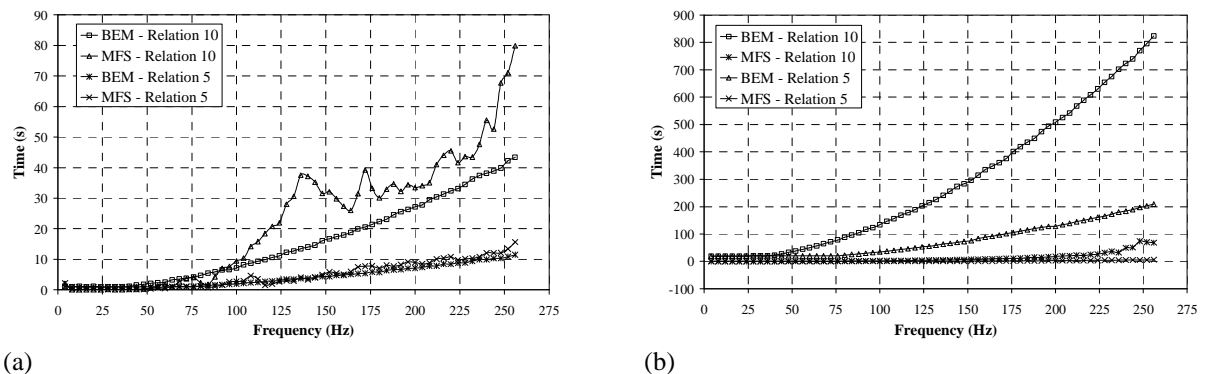


Figure 8: Computation time provided by the numerical models assuming a geometry with a wedge region with: (a) 40m; (b) 200m.

5 NUMERICAL APPLICATION

To illustrate the applicability of the proposed MFS formulation, the problem illustrated in Figure 9 is analyzed in this section. A set of three geometries with varying wedge angles are considered: $\theta = 20^\circ$, $\theta = 10^\circ$ and $\theta = 5^\circ$. For all geometries the depth of the flat region is 20.0 m. The responses were computed for a linear pressure source (S) placed at $y = 19.50$ m, 30.0 m away from the transition between the flat region and the wedge. The acoustic medium is assumed to be water, with a density $\rho_f = 1000.0$ kg/m³ and allowing a dilatational wave velocity of $\alpha_f = 1500.0$ m/s.

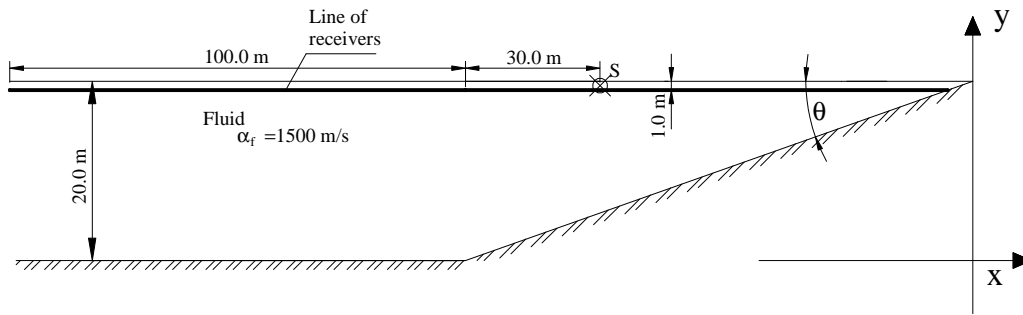


Figure 9: Geometry of the numerical example.

The pressure field generated by the source in the spatial-temporal domain is assumed to be defined by a Ricker wavelet,

$$u(\tau) = A(1 - 2\tau^2)e^{-\tau^2}, \quad (9)$$

where A is the amplitude, $\tau = (t - t_s)/t_o$ and t denotes time; t_s is the time when the maximum occurs, while πt_o is the characteristic (dominant) period of the wavelet. Its Fourier transform is

$$U(\omega) = A[2\sqrt{\pi}t_o e^{-i\omega t_s}]\Lambda^2 e^{-\Lambda^2}, \quad (10)$$

in which $\Lambda = \omega t_o / 2$. This wavelet form has been chosen because it decays rapidly in both time and frequency, thereby reducing computational effort and allowing easier interpretation of the computed time series and synthetic waveforms.

The analysis uses complex frequencies with $\zeta = 0.7\Delta\omega$, which avoid the aliasing phenomena. In the time domain, this effect is later taken into account by applying an exponential window $e^{\xi t}$ to the response (Kausel and Roesset, 1992). The calculations were performed over a frequency range between 2.0 Hz and 1024.0 Hz, assuming a frequency step of 2.0 Hz, which gives a total time of $T = 500.0$ ms. Time domain signals are then computed by means of an inverse Fourier transform. The vertical interface between the flat waveguide and the wedge was modeled using a number of collocation points that was defined according to the excitation frequency of the harmonic source. A ratio of 5 was adopted between the wavelength of the incident waves and the distance between collocation points. The minimum number of collocation points used was 5. The distance between the virtual sources used in the MFS and the boundary was always 10 times the distance between collocation points. Figure 10 displays the time responses along a line of receivers, located 1.0 m below the free surface, for the cases of a flat waveguide (used as a reference) and for the proposed wedge configuration. In the plots regarding the wedge configuration a dashed line was included to mark the beginning of the wedge region. Analysis of these responses allows identifying a sequence of pulses, originated by multiple reflections at the rigid bottom and at the free surface. When the system is composed of a flat waveguide, the response is composed of a first pulse, generated by the source, followed by a sequence of reflected pulses at the top and bottom surfaces. Whenever a pulse impinges on the free surface, its phase is shifted by 180° , inverting its polarity. As time progresses, the wavefront associated with those pulses becomes flatter, generating an almost stationary wavefield.

Comparing the reference case with the wedge configuration, it becomes evident that, in the later, the energy decays much faster, and that the stationary field is not formed, as the energy is scattered away from the wedge. In fact, for all wedge angles, the response at receivers placed above the inclined bottom is limited in the time domain, disappearing after a few reflections on the top and bottom surfaces. As the wedge angle decreases, the responses on the flat region tend to approach that provided by the flat waveguide, although, even for the lowest wedge angle analyzed, it is still possible to identify important differences between both cases, with a considerably lower number of reflections being registered in the time signals.

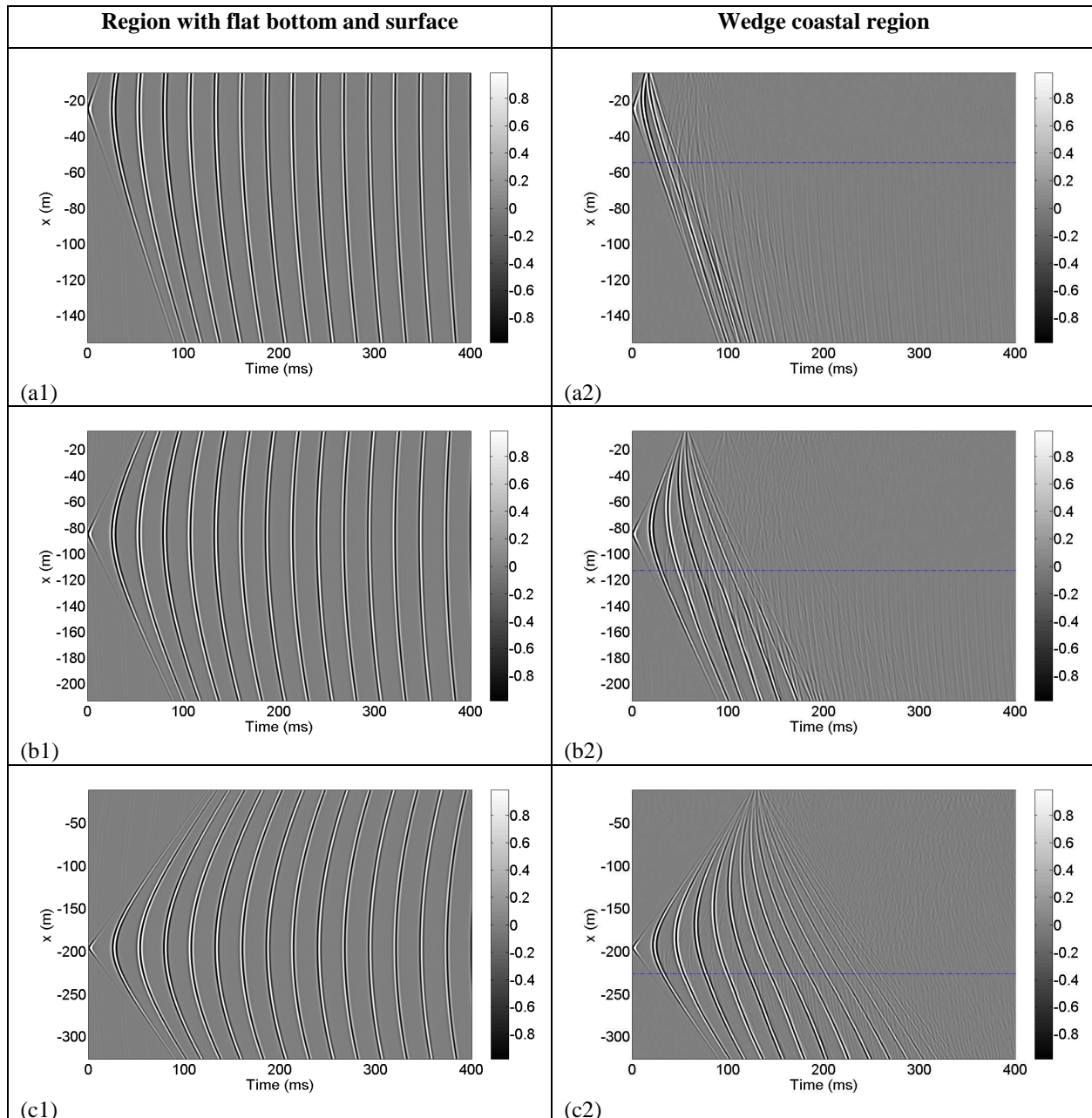


Figure 10: Time domain responses in a wedge coastal region, when the source is placed at position S2 for wedge angles of: (a) $\theta = 20^\circ$; (b) $\theta = 10^\circ$; (c) $\theta = 5^\circ$.

6 CONCLUSIONS

In this paper, the Boundary Element Method and the Method of Fundamental Solutions were used to define numerical frequency domain formulations to simulate the propagation of sound in the vicinity of a wedge costal region, incorporating two sub-regions: one is a flat region with rigid bottom and free surface and the second is a wedge. Appropriate Green's functions were used allowing to reduce discretization. These functions were defined using two approaches: the method of multiple source point reflections was used to model the rigid flat and free surfaces, whereas the response provided by the wedge sub-region was given by a sum of normal modes. The model based on the Method of Fundamental Solutions has proved to be an efficient tool, while still providing accurate results.

A number of numerical examples were presented to illustrate the use of the proposed model in the analysis of underwater wave propagation. In those examples, a flat waveguide coupled to perfect wedges with different apex angles were studied, and relevant differences in the sound propagation patterns could be identified.

ACKNOWLEDGEMENTS

The financial support by FCT (Fundação para a Ciência e Tecnologia) and CAPES (Coordenação de Aperfeiçoamento de Pessoal de Nivel Superior), within the scope of the FCT-CAPES convenium, is greatly acknowledged.

REFERENCES

- Branco, F., Godinho, L., and Tadeu, A., Propagation of pressure waves inside a confined fluid channel with an irregular floor, *Journal of Computational Acoustics*, 10: 183-194, 2002.
- Bouchon, M., and K. Aki, Discrete Wave-number Representation of Seismic Source Wavefields, *Bulletin of the Seismological Society of America*, 67: 259-277, 1977.
- Buckingham, M., and Tolstoy, A., An analytical solution for benchmark problem 1: The "ideal" wedge, *Journal of the Acoustical Society of America*, 87(4): 1511-1513, 1990.
- Cho, H., Golberg, M., and Muleshkov, A., and Li, X., Trefftz methods for time dependent partial differential equations, *CMC: Computers, Materials and Continua*, 1 (1): 1-38, 2004.
- Godinho, L., Tadeu, A., and Branco, F., 3D acoustic scattering from an irregular fluid waveguide via the BEM, *Engineering Analysis with Boundary Elements*, 25: 443-453, 2001.
- Golberg, M. A., and Chen, C. S., The method of fundamental solutions for potential, Helmholtz and diffusion problems, In: *Boundary Integral Methods: Numerical and Mathematical Aspects*, M.A. Golberg (editor), WIT Press & Computational Mechanics Publications, Boston, Southampton, pp. 103-176, 1999.
- Hardin, R.H., and Tappert, F.D., *Applications of the split-step Fourier method to the numerical solution of nonlinear and variable coefficient wave equations SIAM*, 15: 423, 1973.
- Jensen, F.B., Kuperman, W.A., Porter, M.B., and Schmidt, H., *Computational Ocean Acoustics*, American Institute of Physics, Woodbury, NY, 2000.
- Jensen, F. B., and Ferla, C. M., Numerical Solutions of Range-Dependent Benchmark Problems in Ocean Acoustics, *Journal of the Acoustical Society of America*, 87(4): 1499-

- 1510, 1990.
- Kausel, E., and Roesset, J. M., Frequency Domain Analysis of Undamped Systems, *Journal of Engineering Mechanics ASCE*, 118: 721-734, 1992.
- Pekeris, C. L., Theory of propagation of explosive sound in shallow water in: Propagation of Sound in the Ocean, *Geological Society of America, Memoir 27 Geological Society of America*, New York, 1-117, 1948.
- Santiago, J.A.F., and Wrobel, L.C., 2D Modelling of Shallow Water Acoustic Wave Propagation using Subregions Technique, Boundary Element Techniques, International Conference, Queen Mary and Westfield College, University of London, 1999.
- Santiago, J.A.F., and Wrobel, L.C., A Boundary Element Model for Underwater Acoustics in Shallow Water Computer Modeling, *Engineering & Sciences*, 1 (3): 73-80, 2000.
- Santiago, J. A. F., and Wrobel, L. C., Modified Green's Functions for Shallow Water Acoustics Wave Propagation, *Engineering Analysis with Boundary Elements*, 28: 1375-1385, 2004.
- Schmidt, H., and Tango, G., Efficient global matrix approach to the computation of synthetic seismograms, *Geophys. J. R. Astr. Soc.*, 84: 331-359, 1986.
- Stotts, S., Coupled-mode Solutions in Generalized Ocean Environments, *Journal of the Acoustical Society of America*, 111 (4): 1623-1643, 2002.
- Tadeu, A., Pereira, A., and Godinho, L., Three Dimensional Wave Scattering by Rigid Circular Pipelines Submerged in an Acoustic Waveguide, *Journal of Computer Modeling in Engineering and Sciences*, 2(1): 49-61, 2000.
- Tadeu, A., Godinho, L., and António, J., Dynamic response of a three dimensional fluid channel bounded by an elastic floor in the presence of a submerged inclusion via BEM, *Journal of Computational Acoustics*, 13(1): 203-227, 2005.
- Tadeu, A., Santos, P., and Kausel, E., Closed-form integration of singular terms for constant, linear and quadratic boundary elements - Part I: SH Wave Propagation, *Engineering Analysis with Boundary Elements*, 23 (8): 671-681, 1999a.
- Tadeu, A., Santos, P., and Kausel, E., Closed-form integration of singular terms for constant, linear and quadratic boundary elements - Part II: SV-P Wave Propagation, *Engineering Analysis with Boundary Elements*, 23 (9): 757-768, 1999b.